Human Molecular Genetics, 2015, Vol. 24, No. 5 1267–1279

doi: 10.1093/hmg/ddu537
Advance Access Publication Date: 27 October 2014
Original Article

ORIGINAL ARTICLE

Becker muscular dystrophy severity is linked to the structure of dystrophin

Aurélie Nicolas[1,2], Céline Raguénès-Nicol[1,2], Rabah Ben Yaou[3,4,†], Sarah Ameziane-Le Hir[1,2], Angélique Chéron[1,2], Véronique Vié[1,5], Mireille Claustres[6,7,8], France Leturcq[3,9,†], Olivier Delalande[1,2], Jean-François Hubert[1,2], Sylvie Tuffery-Giraud[7,8,†], Emmanuel Giudice[1,2], Elisabeth Le Rumeur[1,2,*], and the French Network of Clinical Reference Centres for Neuromuscular Diseases (CORNEMUS)

[1]Université de Rennes 1, Avenue du Professeur Léon Bernard, 35043 Rennes, France, [2]CNRS UMR 6290, Institut de Génétique et Développement de Rennes, 35043 Rennes, France, [3]Inserm, U974, Université Pierre et Marie Curie-Paris 6, UM 76, CNRS, UMR 7215, Institut de Myologie, Paris 75013, France, [4]AP-HP, Groupe Hospitalier Pitié-Salpêtrière, Centre de Référence de Pathologie Neuromusculaire Paris-Est, Paris 75013 France, [5]CNRS UMR 6251, Institut de Physique de Rennes, Rennes, France, [6]CHU Montpellier, Hôpital Arnaud de Villeneuve, Laboratoire de Génétique Moléculaire, 34000 Montpellier, France, [7]Faculté de Médecine, Université Montpellier 1, 34000 Montpellier, France, [8]Inserm U827, 34000 Montpellier, France and, and [9]AP-HP, Laboratoire de Biochimie et Génétique Moléculaire, Groupe Hospitalier Cochin-Broca-Hotel-Dieu, Paris, France

*To whom correspondence should be addressed at: Institut de Génétique et Développement de Rennes (IGDR), Faculté de Médecine, Avenue du Professeur Léon Bernard, 35043 Rennes Cedex, France. Email: elisabeth.lerumeur@univ-rennes1.fr

Abstract

In-frame exon deletions of the *Duchenne muscular dystrophy* (*DMD*) gene produce internally truncated proteins that typically lead to Becker muscular dystrophy (BMD), a milder allelic disorder of DMD. We hypothesized that differences in the structure of mutant dystrophin may be responsible for the clinical heterogeneity observed in Becker patients and we studied four prevalent in-frame exon deletions, i.e. Δ45–47, Δ45–48, Δ45–49 and Δ45–51. Molecular homology modelling revealed that the proteins corresponding to deletions Δ45–48 and Δ45–51 displayed a similar structure (hybrid repeat) than the wild-type dystrophin, whereas deletions Δ45–47 and Δ45–49 lead to proteins with an unrelated structure (fractional repeat). All four proteins *in vitro* expressed in a fragment encoding repeats 16–21 were folded in α-helices and remained highly stable. Refolding dynamics were slowed and molecular surface hydrophobicity were higher in fractional repeat containing Δ45–47 and Δ45–49 deletions compared with hybrid repeat containing Δ45–48 and Δ45–51 deletions. By retrospectively collecting data for a series of French BMD patients, we showed that the age of dilated cardiomyopathy (DCM) onset was delayed by 11 and 14 years in Δ45–48 and Δ45–49 compared with Δ45–47 patients, respectively. A clear trend toward earlier wheelchair dependency (minimum of 11 years) was also observed in Δ45–47 and Δ45–49 patients compared with Δ45–48 patients. Muscle dystrophin levels were moderately reduced in most patients without clear correlation with the deletion type. Disease progression in BMD patients appears to be dependent on the deletion itself and associated with a specific structure of dystrophin at the deletion site.

† These three authors wish to be considered as representatives of contributors to the UMD-DMD France database.

Received: July 16, 2014. **Revised** and **Accepted:** October 14, 2014

Introduction

The *Duchenne muscular dystrophy* (*DMD*) gene is the largest human gene (79 exons and 2.4 Mb). It encodes the protein dystrophin and is subject to a high number of mutations, with the majority (~70%) being deletions of one or several exons (1). A complete loss of dystrophin due to out-of-frame mutations leads to DMD, a severe and rapidly progressive muscular disease, characterized by early onset and wheelchair (WC) dependency before the age of 13 years (2). In ~1–10 for 100 000 male individuals (3–5), the deletions do not disrupt the reading-frame, and an internally truncated dystrophin is produced, leading predominantly to Becker muscular dystrophy (BMD), an allelic disorder milder than DMD. BMD is clinically heterogeneous with some affected individuals being able to experience a near normal lifestyle and lifespan, while others lose the ability to walk in their late teens or early 20s (6–9). Cardiac involvement is a prominent feature of the disease, and heart failure is the most common cause of early death in BMD patients (10–13).

Dystrophin is a large filamentous protein of 3685 residues and a molecular weight of 427 kDa (14) that protects the sarcolemma from the mechanical stresses of muscle contraction. It belongs to the cytoskeletal family of proteins able to assemble into macromolecular structures with high numbers of protein and lipid partners (15). Dystrophin is composed of four domains: (i) an N-terminal actin-binding domain (ABD1) (approximately exons 1–8); (ii) a central rod-like domain composed of 24 spectrin-like repeats folded in a triple α-helical coiled-coil and connected to the flanking domains by hinges (approximately exons 10–60); (iii) a Cys-rich domain, which links the cytoskeleton to the extracellular matrix via the membrane with a dystrophin-associated glycoprotein complex (approximately exons 61–69); and (iv) the C-terminal end (approximately exons 70–79). We recently characterized the central rod domain using a computational approach and showed that it is organized in separate and putatively specialized functional regions (16).

The central rod domain accounts for >76% of the protein and is the site of the great majority of the deletions that cause BMD (17,18), specifically deletions encompassing exons 44–51 that encode repeats 17–20. Although located in the same gene region, these in-frame deletions are associated with variable clinical severity in BMD patients. It had already been suggested that the cause of this clinical variability could be attributable to structural modifications of dystrophin (12,19,20). However, this hypothesis has never been thoroughly tested.

In this study, we intended to clarify the role of dystrophin structure in the clinical heterogeneity of the BMD patients carrying different in-frame deletions in the mutational hot spot of the *DMD* gene, i.e. deletions of exons 45–47, 45–48, 45–49 and 45–51. We modelled the molecular structures and analysed the biochemical characteristics of the corresponding dystrophins after introducing the deletions into a fragment that includes the repeats 16–21 (R16–21). Concomitantly, we retrospectively collected data measuring cardiac and motor function in a large cohort of French BMD patients bearing these four deletions. A semi-quantitative assessment of dystrophin levels was also collected in about half of the patients. The analysis of clinical, modelling and biochemical data provide clear evidence that the structural characteristics of dystrophin at the deletion site are strongly associated with phenotype severity in BMD patients. Notably, Δ45–48 and Δ45–51 deletions, which exhibit structural features similar to wild-type protein at the deletion site, are associated with a slower disease progression compared with Δ45–47 or Δ45–49 deletions which both lead to profound structural modifications of dystrophin.

Results

Molecular modelling of the internally truncated proteins shows hybrid versus fractional repeats at the deletion site of dystrophin

All models (Fig. 1) were assessed using PROCHECK (22), which calculated the values of the Φ/Ψ dihedral angles of the peptide bond for each residue (i.e. the Ramachandran plot) within the atomic models. Most of the residues of the initial models were in the most energetically favoured regions while <2% of residues were in energetically unfavoured regions (Table 1). These last residues were situated in loops regions that are highly dynamic and thus with a structuration more difficult to predict by homology modelling. Overall, these data showed that the models were of high quality. As shown by molecular homology modelling (16) and crystallography (23), each dystrophin repeat is composed of three helices, A, B and C, which form a triple helical coiled-coil (Fig. 1, inset). The four truncated dystrophin exhibited modified structures compared with the wild-type R16–21. They all bear deletions starting at exon 45, which encodes the C terminal half of repeat 17 that is therefore lacking in all studied deletion mutants. However, two types of structures were observed at the deletion site, namely hybrid or fractional repeats (18). Hybrid repeats with structure similar to triple coiled-coil repeat structure at the deletion site were observed in RΔ45–48 and RΔ45–51 (with and without hinge 3, respectively). Fractional repeats that do not reconstitute a native triple coiled-coil repeat at the deletion site were observed in RΔ45–47 and RΔ45–49 (both with hinge 3).

To assess the stability of these models, molecular dynamics (MD) relaxation was performed. The root-mean-square deviation (RMSD; see Materials and Methods for definition) of the Cα atoms was measured and showed that the models reached equilibrium for the last 22 ns of the MD trajectory (Supplementary Material, Fig. S1). The repeats globally maintained their tridimensional structures as showed by their Φ/Ψ dihedral angles with an increase of residues situated in the energetically favoured regions of the Ramachandran plots (Table 1). The number of residues in energetically unfavoured regions decreased substantially after the MD relaxation indicating an increase of the global quality of the models. The analysis of the fluctuations by the root-mean-square of fluctuation (RMSF; see Materials and Methods for definition) (Supplementary Material, Fig. S2) of each Cα atom along the sequence showed that all the models maintained their secondary structures, helices and loops. By analysing the conformational clustering (Supplementary Material, Fig. S3), it was evident that the models presented specific points of flexibility shown by arrows in Figure 2A. A flexibility spot was located for the R16–21 wild-type model at the junction between the repeats 18 and 19. Remarkably, the flexibility of the two fractional repeats was enhanced at the deletion sites themselves, indicating that these sites represent points of structural weakness. This contrasted with the two deleted proteins exhibiting hybrid repeats, as

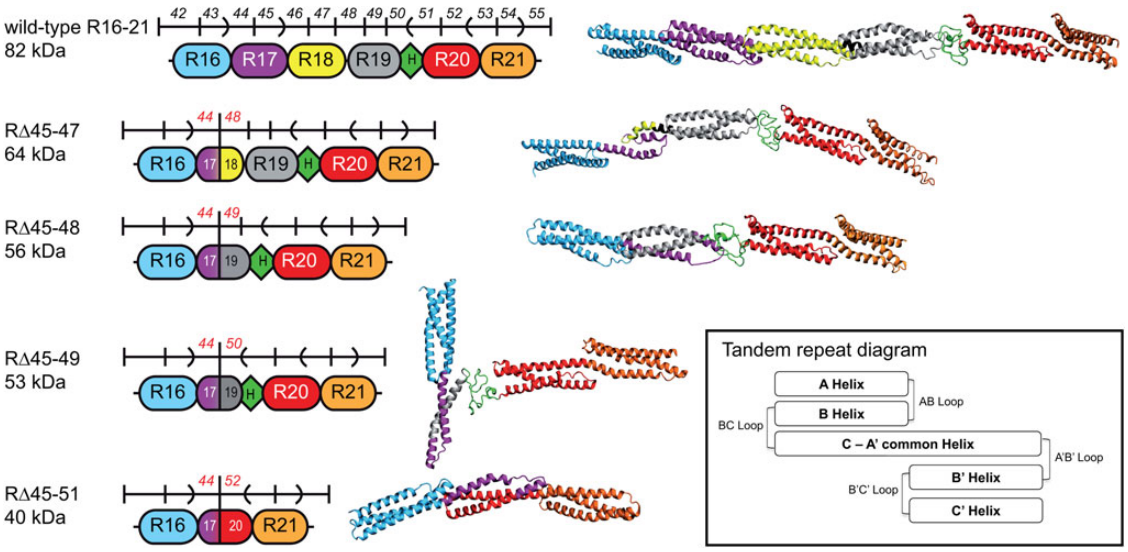

Figure 1. Structural consequences of the exon deletions obtained by *in silico* molecular homology modelling. Schematic representation of the exons and their corresponding encoded proteins of interest, with their molecular weight. On the top of each drawing, the exons are noted by their numbering: a vertical bar indicates an 'in-frame' succession of repeats while the '>' sign indicates an 'out-of-frame' succession of exons. The new bounded exons around a deletion are indicated in red. Repeats are coloured and numbered according to the alignment from Winder (21). The green diamond represents the hinge 3. Molecular homology models are shown on the right of the schematic representation of proteins (cyan: R16, purple: R17, yellow: R18, grey: R19, red: R20, orange: R21). An inset shows that a tandem repeat is made of three helices (**A–C**) joined by loops and structured in a coiled-coil; the continuity of the filament is obtained by the common helix containing the C-helix of the first repeat followed by the A′-helix of the following repeat. In the R16–21 model, each wild-type repeat has three α-helices gently wrapped in a coiled-coil. This filamentous structure is interrupted by the presence of hinge 3 in green. Models of the four truncated proteins are presented with the repeats coloured as in the wild-type R16–21. The truncated proteins all bear deletions starting at exon 45, which encodes the C-terminal half of repeat 17. The RΔ45–47 protein lacks part of repeats 17 and 18 and forms a structure clearly different from a true repeat at the site of the deletion. This incomplete repeat is known as a 'fractional repeat'. RΔ45–48 is lacking part of repeat 17, all of repeat 18 and part of repeat 19 and a structure similar to a true repeat is formed at the site of the deletion, with three helices forming a new coiled-coil called 'hybrid repeat'. RΔ45–49 is truncated from the middle of repeat 17 to the middle of repeat 19, and the two remaining parts of repeats 17 and 19 form two helices wrapped in a double coiled-coil; as the third helix of a conventional repeat is lacking in this mutant, the directionality of the molecule at the junction with hinge 3 is changed. This mutant therefore bears a 'fractional repeat' with a non-filamentous topology. RΔ45–51 lacks part of repeat 17 and all of repeats 18 and 19 and hinge 3; the remaining parts of repeat 17 and of repeat 20 make a 'hybrid repeat'.

Table 1. Distribution of the residues (%) in the dihedral Ψ/Φ angles values of the Ramachandran plot regions

Proteins	Models	Energetically favoured region*	Energetically moderately favoured region**	Energetically unfavoured region***
R16–21	Initial model	98	0.8	1.2
	After MD	98.6	1.4	0.0
RΔ45–47	Initial model	97	1.0	2.0
	After MD	98.2	1.4	0.4
RΔ45–48	Initial model	97.1	1.6	1.3
	After MD	98.7	1.3	0.0
RΔ45–49	Initial model	96.9	1.4	1.7
	After MD	99.1	0.5	0.5
RΔ45–51	Initial model	97.8	0.6	1.6
	After MD	99.1	1.0	0.6

*, ** and ***corresponding to the classical Ramachandran core and allowed *, generously allowed ** and disallowed *** regions.

the RΔ45–48 structure showed flexibility at the hinge 3 region, while RΔ45–51 exhibited a remarkably stable structure (no arrow).

Molecular descriptors of the truncated dystrophins compared with wild type

The electrostatic potential and molecular hydrophobicity potential (MHP) profiles of the truncated dystrophins were profoundly modified compared with wild-type dystrophin. The electrostatic potential at the C-terminal region of the new junction site differed dramatically from one protein to another (Fig. 2B), without specific variations corresponding to hybrid or fractional repeats. The sequence predicted isoelectric point p*I* increased from 5.38 for the wild type to 6.32 for the RΔ45–51 (Fig. 2C) showing that an identical N-terminal region was joined to a C-terminal region with increasing cationic properties as the deletion size increased. In contrast, the variations in the MHP were related with the hybrid or fractional structure type at the deletion site (Fig. 2D and E). Clearly, a higher hydrophobic surface was exposed to the solvent in fractional repeats compared with hybrid repeats. In the fractional repeat-containing proteins, whether composed by small helices (RΔ45–47) or by a double coiled-coil (RΔ45–49), hydrophobic residues normally buried in the wild-type repeats were largely exposed to the surface. For the hybrid repeat-containing proteins, the hydrophobic residues buried in the wild-type protein remained buried even though the facing residues inside the coiled-coil were modified due to the deletions.

Biochemical characterization of wild-type and truncated dystrophin

To understand how the structure modifications observed on the molecular models could be related to the biochemical and

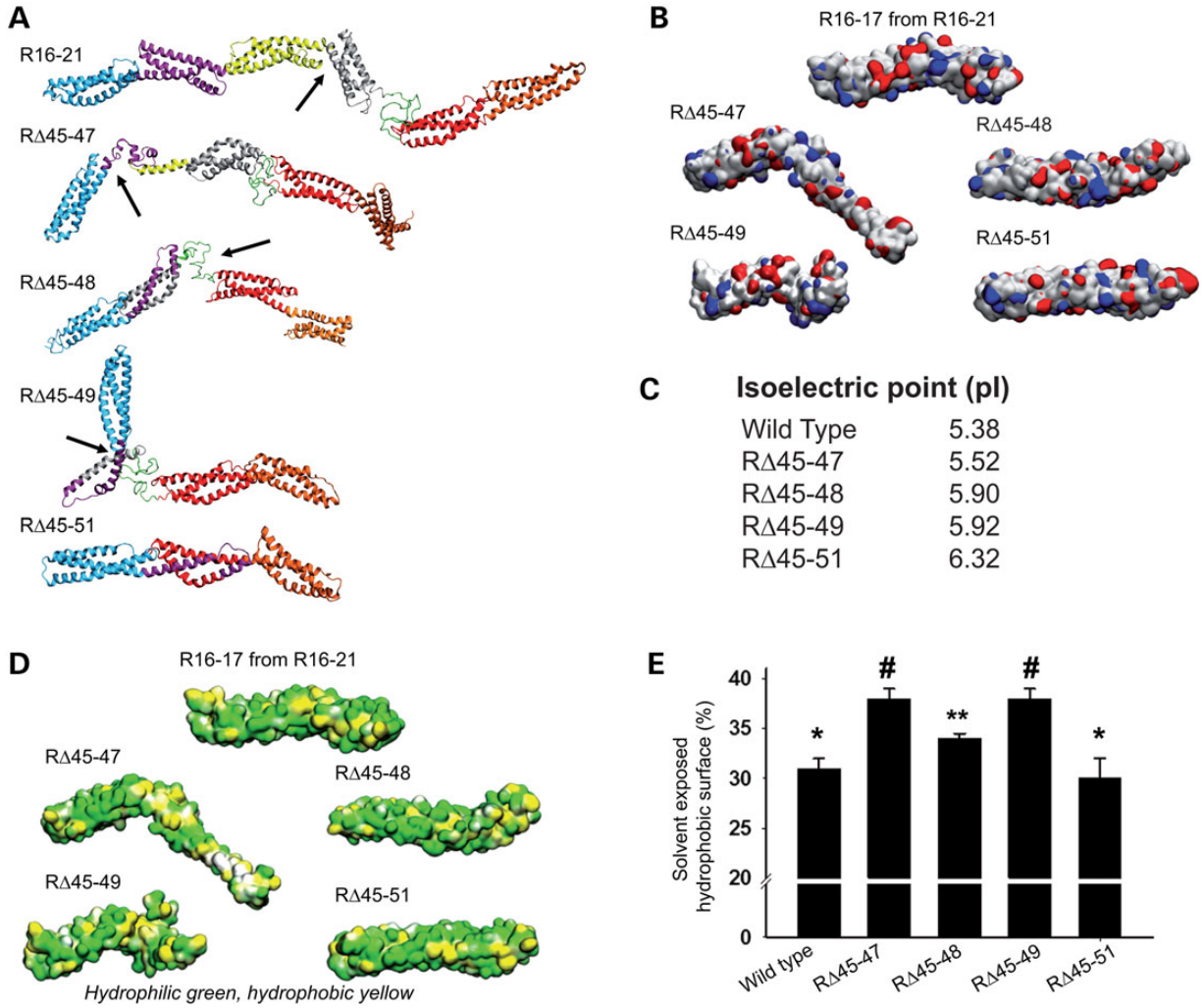

Figure 2. Analysis of the MD relaxation of the five homology models. After 22 ns of molecular relaxation, the most representative model of each protein is showed (colour code similar to Fig. 2). Specific points of flexibility are indicated (arrows). The wild-type R16–21 shows a point of flexibility at the R18–19 linker, whereas RΔ45–47 and RΔ45–49, structured in fractional repeats, shows high flexibility at their respective deletion sites. The two hybrid repeats of RΔ45–48 and RΔ45–51 maintain their initial structures, with the RΔ45–48 tending to fluctuate at the region linking repeat 19 to hinge 3. (**B**) Electrostatic potential projected on the solvent-accessible surface of the wild type and the truncated dystrophins. Each model was coloured using the APBS electrostatic potential calculated for an ionic strength of 50 mM and the surface colours were clamped at −3 (red) and +3 (blue) kTe^{-1}. Only the regions around the deletion site and corresponding to repeats 16–17 (R16–17) of the wild-type are shown. (**C**) Isoelectric points were calculated using primary sequences. (**D**) MHP were obtained from PLATINUM server and displayed using VMD. The hydrophobicity scale is green–white–yellow, with green representing the most hydrophilic regions and yellow the most hydrophobic. Only the regions focused in (B) are shown. (**E**) Mean solvent exposed hydrophobic surface ± SD of the three clusters obtained by MD (% of the total surface). * and #, the values are identical from each other and different from the other ($P < 0.05$); **, the value is different from all other values ($P < 0.05$).

biophysical properties of the proteins, they were expressed in *Escherichia coli* (Table 2). All were obtained with degrees of purity close to 95%, as determined by SDS–PAGE (Fig. 3A).

Truncated proteins are folded into coiled-coils like wild-type dystrophin

To examine the effect of the deletions on the secondary structure of dystrophin, the wild-type and truncated dystrophins were analysed using circular dichroism (CD). All of the structures had typical CD spectra with two minima at 208 and 222 nm. The values at 222 nm indicated α-helix contents that ranged between 50 and 75%. Interestingly, the CD spectra showed that the ratio of the molar ellipticity at 222 and 208 nm was ≥1 for all proteins, meaning that all the proteins were folded predominantly into coiled-coils (24) (Fig. 3B).

The truncated proteins remained highly stable compared with wild-type dystrophin

To determine if the deletions induce modifications in stability, thermal heating was followed by CD at 222 nm, and chemical denaturation by urea was followed by tryptophan intrinsic fluorescence. Thermal heating and urea denaturation revealed typical sharp two-state transitions for all of the proteins. The highest thermal mid-denaturation at 66 ± 0.8°C was recorded for wild-type R16–21. Similar values were observed for the truncated proteins RΔ45–47 and RΔ45–48 at 65°C, and lower values at 61°C were measured for RΔ45–49 and RΔ45–51 (Fig. 3C). The wild-type R16–21 protein displayed a mid-denaturation at 5.2 M urea. A similar behaviour was observed for the truncated protein RΔ45–47, while mid-denaturation was achieved with lower urea concentration for the three other proteins (4.9–5 M of mid-denaturation) (Fig. 3D). However, the wild-type protein exhibited the highest

Table 2. Sequence and molecular weight of the wild-type R16–21 and the four truncated proteins

Protein (number of residues)	First residue	Last residue	N-terminus sequence	C-terminus sequence	Molecular weight (kDa)
R16–21 wild-type (706)	1991	2694	LEISYV. . .	. . .ETHRLLQQF	82
	Residue in N terminal of the deletion	Residue in C terminal of the deletion	Sequence of the junction of the deletion	Molecular weight (kDa)	
RΔ45–47 (548)	2146	2305	. . .WYLKVSRA. . .	63.9	
RΔ45–48 (486)	2146	2365	. . .WYLKETEI. . .	56.7	
RΔ45–49 (452)	2146	2401	. . .WYLKRKLE. . .	52.9	
RΔ45–51 (338)	2146	2515	. . .WYLKATMQ. . .	40.1	

stability, indicating that protein length and the presence of hinge 3 do not preclude stability. We can conclude that the two truncated proteins RΔ45–47 and RΔ45–48 were roughly as stable as wild-type R16–21, whereas the two shorter truncated proteins showed slightly decreased stability compared with the full-length fragment. However, compared with point mutations that modify the sequence, these four proteins obtained by joining non-neighbouring regions of the wild-type protein were highly stable, consistent with previous studies demonstrating that this region of the dystrophin central domain is highly stable compared with the more proximal region such as this of repeats 1–3 (25) and remained highly stable even after the exon coded sequence deletions.

Refolding properties after urea denaturation are highly modified in the truncated dystrophin fragments compared with the full-length R16–21 protein

Refolding after denaturation is a critical dynamic parameter. Refolding after 8 M urea denaturation of the full-length and the three truncated proteins RΔ45–47, RΔ45–49 and RΔ45–51 was described by mono-exponential fits. The fastest mono-exponential refolding rate constant at $10.6 \pm 2.9\ s^{-1}$ was observed for the RΔ45–51 truncated protein ($P < 0.0001$) (Fig. 3E). The two other truncated proteins RΔ45–47 and RΔ45–49 displayed slower refolding rate constants of 4.3 and $3.0\ s^{-1}$, respectively. Interestingly, the refolding of RΔ45–48 was better described by two exponential components, one corresponding to a fast phase at $12.4 \pm 4.4\ s^{-1}$ and one to a slower phase at $2.3 \pm 0.6\ s^{-1}$, each of them contributing approximately half of the total amplitude. The fast component was similar to the refolding rate constant of the truncated protein Δ45–51, and the slow rate constant was the slowest rate reported. The refolding rate constant of wild-type R16–21 was intermediate at $5.7 \pm 0.7\ s^{-1}$. This value was significantly different from all other values, indicating that refolding is not slowed by the length of the protein. However, the fastest value was reported for the shorter truncated protein RΔ45–51, the only fragment lacking hinge 3, indicating that the presence of hinge 3 could slow down the refolding process. Clearly, the two truncated proteins RΔ45–47 and RΔ45–49 display slower global refolding than the other truncated proteins. The refolding rates of the truncated proteins were linearly and inversely correlated with the increases in the percentage of the hydrophobic surface exposed to solvent ($R = 0.98$, not shown). Indeed, the solvent exposure of some hydrophobic residues that were buried in the wild-type protein slowed down the refolding process. The refolding rates and MD data suggested that hybrid and fractional repeats could be distinguished by their dynamic properties. The refolding rates indicated that the fractional repeats required additional time to find the correct fold compared with the wild-type and to hybrid repeat-containing proteins. These observations were in agreement with the MD results, which indicated that fractional repeats had topologies and properties far different from those of the wild-type and hybrid repeat-containing proteins.

Age of DCM onset and of WC dependency of the BMD patients

From an initial cohort of 251 French patients carrying one of the four studied deletions Δ45–47 (127 patients), Δ45–48 (90 patients), Δ45–49 (31 patients) and Δ45–51 (3 patients) (Table 3), we were able to compare the clinical outcome in a subset of 106 patients aged >16 years for whom the ages of onset of DCM and/or WC dependency were known: Δ45–47 ($n = 50$), Δ45–48 ($n = 38$) and Δ45–49 ($n = 18$). Among them, 18 patients exhibited both DCM and WC dependency (Supplementary Material, Table S1).

Our data showed a significant difference towards earlier DCM onset in Δ45–47 BMD patients (median age of 27 years) compared with Δ45–48 patients (median age of 38 years, $P = 0.031$) or Δ45–49 BMD patients (median age of 41 years, $P = 0.042$) (Fig. 4A). In addition, we observed that WC dependency exhibited a clear trend toward affecting Δ45–48 BMD patients at an older age than Δ45–47 BMD patients, with a delay of 11 years (median ages of 49 and 38 years, respectively), although this difference did not reach statistical significance ($P = 0.082$) (Fig. 4B). Conversely, Δ45–49 BMD patients became WC confined at a similar median age (35 years) as Δ45–47 patients (38 years, $P = 0.416$) but 14 years earlier than Δ45–48 patients (49 years, $P = 0.029$). These differences clearly indicated that the severity spectrum was shifted toward slower disease progression for Δ45–48 BMD patients compared with Δ45–47 and Δ45–49 BMD patients. Δ45–51 patients could not be discussed here as none of the three patients in the original cohort were WC confined or DCM affected.

Dystrophin expression levels in BMD patients

When available in this retrospective cohort study, dystrophin amounts from western blots (WBs) were classified into four levels (normal, high, medium and low). Data were available for 79 of the 239 patients bearing one of the four deletions in the initial cohort and showed that most of them displayed a medium level of dystrophin, while the sixth of patients displayed low, high or normal levels for each of the deletions (Fig. 4C). When considering only the patients with DCM or WC bound, they also displayed mostly

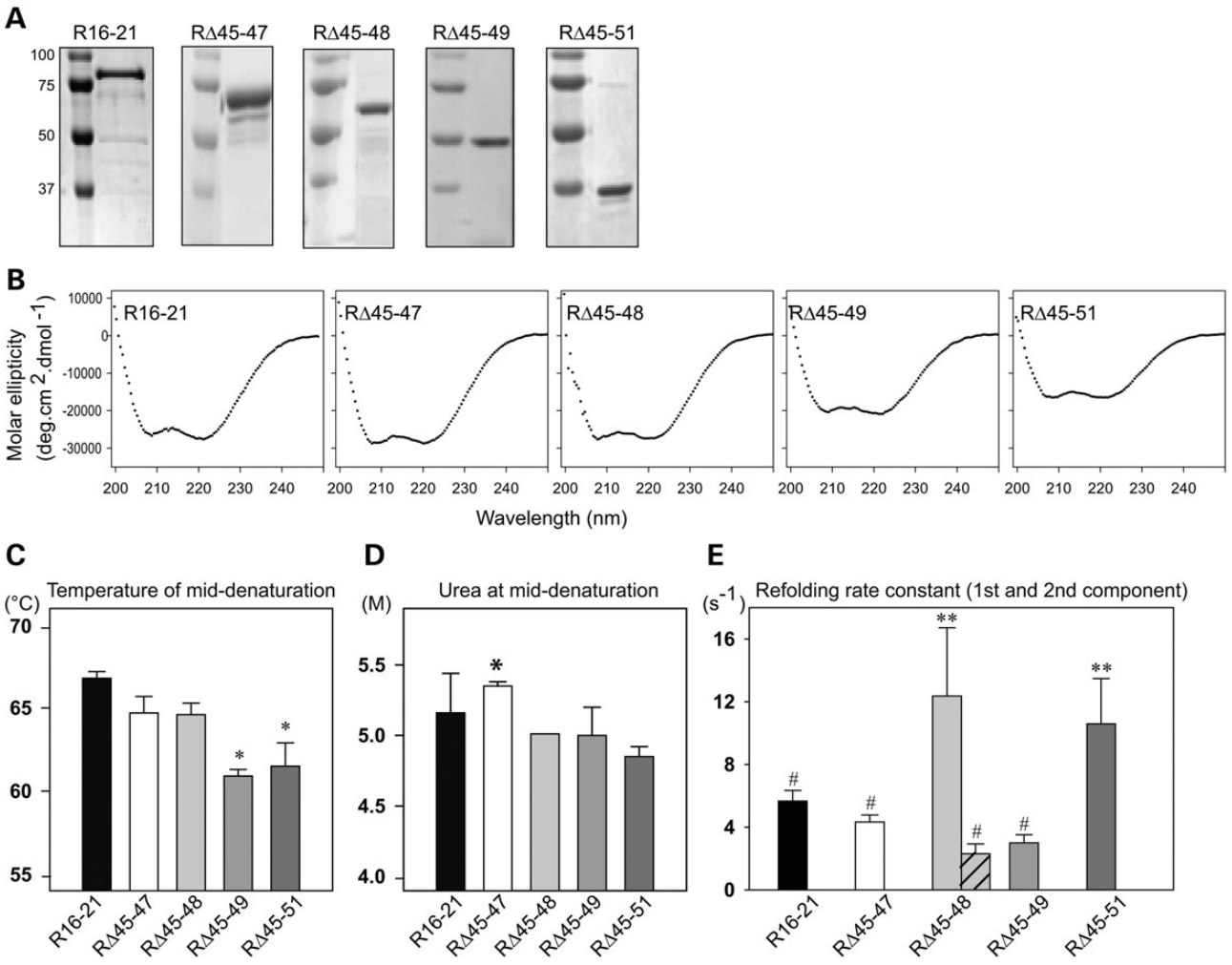

Figure 3. Biochemical consequences of the exon deletions compared with wild type. Proteins were expressed in *E. coli* and further purified by affinity chromatography. (**A**) SDS–PAGE of the five proteins revealed by Coomassie blue staining. Molecular weight markers are on the left side of the gels. Protein purity is over 95%. (**B**) CD spectroscopy performed with wild-type R16–21 and the four truncated proteins. The spectra of the molar ellipticity versus wavelength showed two minima at 208 and 222 nm, as expected for proteins folded in α-helices. (**C**) The temperature at mid-denaturation and (**D**) urea at mid-denaturation are plotted. Values are reported as the mean ± SD of at least three measures. *, values similar and different from all other values (t-test, $P < 0.05$). (**E**) Refolding rate constants were measured by stopped-flow fluorescence. Proteins unfolded in 8M urea were 10-fold diluted in urea-free buffer and intrinsic tryptophan fluorescence was monitored. Values represent exponential rate constant ± SD for at least five experiments. #, values significantly different from all other values (t-test, $P < 0.05$); **, values identical and significantly different from all other values ($P = 0.0001$).

medium levels of dystrophin. Only four patients with Δ45–47 and one with Δ45–48 had low levels of dystrophin while seven patients with Δ45–48 and three patients with Δ45–47 had high or normal levels of dystrophin (Fig. 4D).

Discussion

By combining several approaches including (i) in-depth structural and biochemical investigations of truncated dystrophin molecules and (ii) clinical assessment in large subsets of French BMD patients with identical mutations, we provided clues about the role of the structure of dystrophin at the deletion site on disease progression in patients carrying in-frame deletions in the central rod domain of the protein. Clearly, refolding rates and molecular simulations data suggested that hybrid and fractional repeats could be distinguished by their dynamic properties.

The heterogeneity of the BMD phenotype has long been investigated. Whereas in-frame deletions in the N-terminal actin-binding domain or in the CYS-rich domain were reported to result in a more severe clinical outcome (6,17), phenotype in patients carrying deletions in the central rod domain of dystrophin was more variable, ranging from isolated elevated blood creatine phosphokinase and cramps to classical BMD (6,9,26). Although the reasons for this variability are not fully understood, it is likely that both levels and functionality of the internally deleted dystrophins play a significant role (27–29).

Most BMD patients have reduced dystrophin expression levels, the milder phenotypes being associated with the higher expression levels (27). Thus, as high as 75% of normal dystrophin expression is found in patients with the very mild Δ45–51 deletion (27,30), and asymptomatic patients have significantly higher dystrophin expression levels compared with symptomatic BMD patients (26,27,31). In our cohort, the majority of BMD patients were classified as having medium level of dystrophin expression. However, dystrophin amounts were heterogeneous between patients carrying different deletions but also between patients carrying the same deletion as previously shown (6,8,26,27,30,32,33), and did not correlate with the age of onset of DCM or of WC

Table 3. Description of the French BMD patients' cohort

Deletions (number of patients)	Mean age in years (age range)	Number of patients with DCM or not (% of the number of patients) (number of patients with known age of onset)			Number of patients using WC or not (% of the number of patients) (number of patients with known age of onset)				Patients with both DCM and WC permanent use (% of the number of patients)
		Yes	No	Unknown	Always	Partial	None	Unknown	
Δ45–47 (127)	46 (17–79)	40 (32%) (35)	58 (47%)	27 (21%)	23 (18%) (18)	15 (13%)	85 (67%)	2 (2%)	6 (5%)
Δ45–48 (90)	47 (18–83)	34 (38%) (31)	38 (42%)	18 (20%)	15 (17%) (12)	8 (9%)	65 (72%)	2 (2%)	5 (6%)
Δ45–49 (31)	49 (20–80)	17 (55%) (14)	9 (29%)	5 (16%)	14 (45%) (11)	5 (16%)	11 (36%)	1 (3%)	7 (23%)
Δ45–51 (3)	25 (20–31)	0	2	1	0	1	2	0	0

Partial WC use includes patients who are still ambulant but are using a WC for long distances or only outdoors. The 'Unknown' status corresponds to those patients for whom no recently updated neurologic or cardiologic data are available.

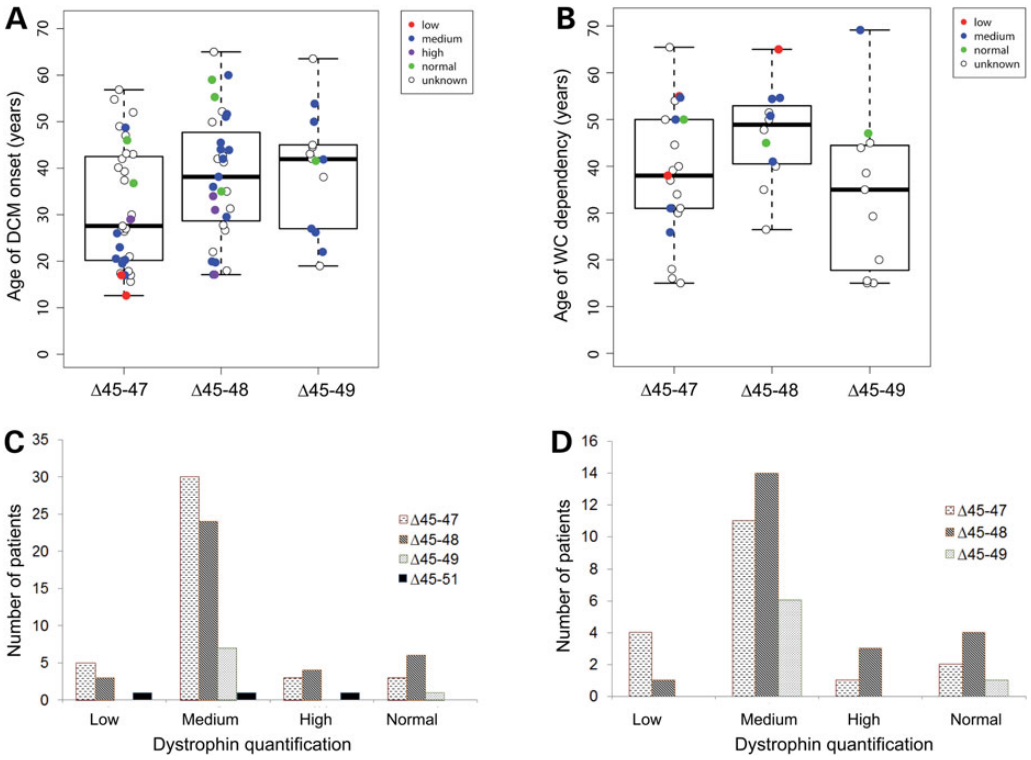

Figure 4. Ages of DCM onset and WC dependency and dystrophin expression levels from the Δ45–47, Δ45–48, Δ45–49 and Δ45–51BMD patients. Dots indicate the individual age of DCM onset or WC dependency, and boxes indicate the location of 50% of the individual values. Horizontal bars indicate the median age in years. Coloured/wide dots indicated the dystrophin expression level class of each patient as shown in the inset. (**A**) Box plot and dot plot distributions of age of DCM onset versus deletion type. Analysis of variance (ANOVA) revealed a statistically significant difference between groups ($P = 0.036$). The Mann–Whitney test revealed a significant difference in the median ages of DCM onset in Δ45–48 and the Δ45–49 BMD patients which were 11 years ($P = 0.031$) and 14 years ($P = 0.042$) later, respectively, than the median age of DCM onset in Δ45–47 BMD patients. (**B**) Box plot and dot plot distributions of age of WC dependency. ANOVA showed a non-significant P-value of 0.088. However, the median age of WC dependency was 14 years later in Δ45–48 patients than Δ45–49 BMD patients ($P = 0.029$ by the Mann–Whitney test). Although the difference was not statistically significant ($P = 0.082$ by the Mann–Whitney test). WC dependency tended to occur at an earlier age in Δ45–47 patients (median age, 38 years) compared with Δ45–48 patients (median age, 49 years). (**C** and **D**) Dystrophin amounts are reported after semi-quantitative inspection of WB. By comparison with control normal muscle extracts, the levels were categorized into four classes: normal (~70–100% of control amount), high (~50–70% of control amount), medium (~10–50% of control amount) and low (<10% of control amount) (see also Supplementary Material, Table S2). The number of patients per class and per deletion type were reported. (C) Dystrophin amounts for all the BMD patients of the cohort whatever the cardiac and muscle status. (D) Dystrophin amounts for the patients of A and B.

dependency. Measuring dystrophin levels accurately remains highly challenging (34) and the levels may be variable within a single myofiber, between adjacent myofibers and muscle biopsies. It has also been proposed that at expression levels <75% and >30%, the structural characteristics of the internally deleted dystrophins could play a significant role in the phenotype (35). This assumption was consistent with a recent study showing that there is no linear correlation between dystrophin levels and disease severity in BMD patients, notably those carrying a Δ45–47 deletion: as long as dystrophin level is above a threshold (estimated to be ~10%), the mutation is likely an important factor in determining disease severity (33).

Previous studies that aimed to explore the underlying rationale of clinical variability in BMD patients were mostly based on the analysis of heterogeneous groups of patients carrying different types of deletions even though located in the same gene region: patients with distal versus proximal deletions or in the centre of the dystrophin central rod domain (6,8,26,32), those

with deletions ending at specific exons (12,31) or with deletions including or omitting hinge 3 (12,36). Very often patients were relatively young and still ambulatory, and the cardiac status was not reported. Overall, the obtained data suggested that the central region is not completely homogenous with respect to function, but did not allow to support a clear view of genotype–phenotype correlations in BMD patients having deletions in the central rod domain of dystrophin.

The methodology used here to address this question was based on the retrospective analysis of large subsets of BMD patients bearing identical deletions for whom two readily comparable and robust items as markers of disease severity (age of DCM and WC dependency) could be obtained. A comparison analysis was performed between clinical outcome in patients bearing Δ45–47, Δ45–48, Δ45–49 and Δ45–51 deletions and the predictive functionality of the truncated proteins based on the molecular properties of hybrid versus fractional repeats at the deletion site compared with wild type. The concept of hybrid repeat is reminiscent of the phasing of the repeats in mini- or micro-dystrophins studied by Harper *et al.* (37). They showed that the mini-dystrophin ΔH2-R19 containing eight perfectly phased repeats significantly improved *mdx* mouse muscle function compared with the closely related construct with a deletion of the exons 17–48. This deletion was originally observed in a patient (38) and contains 'non-phased' repeats that give rise to a fractional repeat according to our predictions. Specific attention was drawn to repeats phasing in the design of the subsequent studies with mini- and micro-dystrophins in *mdx* mouse or *grmd* dog (39–41). The most popular micro-dystrophin is the ΔR4–R23/ΔCT which is perfectly phased (42,43). However, the mini-dystrophin ΔH2-R19 was reported to be prone to aggregation in an *in vitro* assay (44) emphasizing the idea that the presence of non-native inter-repeat junction could partly compromise the dystrophin function. Quite differently, the presence of hybrid or fractional repeats at the deletion site (19,20) are due to the fact that the B-helices of all the repeats except repeat 14 are encoded by two successive in-frame exons, with their boundaries precisely aligned with the third heptad of the B-helices (18). Thus, a deletion that maintains the coding of a B-helix by two exons around the deletion site allows for the formation of a hybrid repeat similar to a true repeat. This type of deletion maintains the heptad pattern of the residues along the primary sequence (21) and allows hydrophobic residues to be localized inside the coiled-coils which favours a fast refolding. In contrast, in case of a deletion that leads to a fractional repeat, hydrophobic residues are not folded inside a coiled-coil but remain accessible to the solvent, slowing down the refolding process and constituting sites of weakness in dystrophin. Both hybrid and fractional repeats at the deletion sites did not decrease dramatically the protein stability indicating that overall the dynamical properties were of highest importance for the function of dystrophin. This was not striking since dystrophin is primary involved in the resistance to the stress of elongation in muscle cells (45,46). However, the deletions that lead to hybrid repeats had the least impact on the structure of dystrophin, even if hinge 3 was also deleted. Kaspar *et al.* (12) anticipated the rule of hybrid versus fractional repeats, which they called in-phase and out-of-phase repeats, respectively. They suggested that the topology of the truncated protein produced by Δ45–47 reversed the direction of the filament. In contrast, here we showed a topology that remained filamentous in RΔ45–47, even though there was an incomplete coiled-coil structure at the deletion site. Indeed, in Kaspar *et al.* previous study, mutated models were manually constructed considering that each repeat contained both a long and a short helix. This was not in line with the clear features now available from the X-ray crystals of spectrin and dystrophin repeats, which showed that repeats are made of three helices gently wrapped in a coiled-coil (47). Therefore, our data argued for a conserved filamentous structure in RΔ45–47 and a profoundly modified topology of RΔ45–49. Finally, we showed here that it is not the absence of hinge 3 that correlated with the age of onset of DCM (12) but the structure of these truncated dystrophins.

According to the structural and dynamic modifications observed in the various internally truncated mutants studied, we suggested a functional classification such that R16–21 > RΔ45–51 > RΔ45–48 > RΔ45–47 ~ RΔ45–49, that is partly dependent on the presence of hybrid versus fractional repeats at the deletion sites.

Is this classification relevant at the biological and clinical levels?

The analysis of our cohort of patients allowed clear trends for cardiac and/or motor severity to be established depending on the truncated protein structure. We showed that severity gradation among the four most frequent BMD deletions increases from Δ45 to 51, through Δ45–48 and up to Δ45–47 and Δ45–49, with Δ45–48 patients being affected by DCM 11 years later than Δ45–47 patients and patients with Δ45–47 and Δ45–49 being at risk to be WC-dependent 11–14 years earlier than patients with Δ45–48. These observations strongly correlated with the presence of hybrid repeats at the deletion sites in the RΔ45–51 and RΔ45–48 truncated proteins and with the presence of fractional repeats at the deletion sites of the RΔ45–47 and RΔ45–49 truncated proteins. Because RΔ45–51 is the truncated protein the most similar to wild type, it is tempting to correlate this similarity with the characterization of Δ45–51 as a clinically very mild deletion (48) with a dystrophin expression level of ~75% of wild type (27,30). The lack of symptoms may explain why such a small number of Δ45–51 carriers was present in the UMD-DMD database. Although Δ45–48 displayed a hybrid repeat, the increased flexibility of this variant compared with the wild-type and Δ45–51 proteins could partly impair the binding of the actin-binding domain 2 (repeats 11–17) to filamentous actin (49) thereby explaining why the Δ45–48 phenotype is so different from the very mild phenotype of Δ45–51. The Δ45–47 and Δ45–49 deletions lead to fractional repeats at the deletion site, which we demonstrated to constitute structurally weakened sites compared with hybrid repeats. Whether the dynamic properties associated with the hybrid or fractional repeats are relevant *in vivo* remains speculative, but the folding of this long filamentous protein *in vivo* is probably a rather complex process, and thus deletions that partly impair or slow down this process could be deleterious.

These results reinforced the idea that the 'phasing' of the repeats provides improved function to truncated dystrophin (12,19,20,37,44). This hybrid repeat phasing appears to be essential for the function of dystrophin as a molecular shock absorber, protecting the membrane from the stresses of contraction (45,46,50). In contrast, the fractional repeats are less able to protect membrane from the stresses due to their structurally weakened deletion sites.

Single-exon reported BMD deletions produce fractional repeats (18), although some of them have been associated with mild phenotypes, which is not in agreement with the results of this study. The structures of such truncated dystrophins remain to be studied in detail, and the results could depend on the region of the central domain of dystrophin involved in. Indeed, the proximity of a hinge, such as for the deletion of exon 16, or the loss of the binding motif for an interacting partner, could also play a role in the severity of the resulting phenotypes (51,52). In that sense,

the region covering repeats 16–21 was involved in nNOS binding (53,54). For patients with the mild deletion Δ45–55 (55), the mislocalization of nNOS was a worsening factor (56) even though this deletion was predicted to lead to a hybrid repeat structure of dystrophin.

This showed that other factors are likely able to modulate the severity of the phenotype associated with a deletion leading to a hybrid repeat-containing protein, and may also account for the intra- and intergroup variability. These factors may include *cis*-acting elements such as spontaneous alternative splicing events occurring in a fraction of dystrophin transcripts (57), the presence of non-synonymous SNPs, notably those reported in the exons encoding the central rod domain of the protein (58), posttranscriptional regulation by microRNA (59), but also other genetic modifiers of disease severity (60–63).

In conclusion, our findings further support a significant role of the structure of the internally truncated dystrophins produced by in-frame deletions in the central rod domain of dystrophin in determining disease severity in BMD patients. We showed that the severity of the BMD phenotype could be regarded as deletion specific. Indeed, exon deletions leading to hybrid repeats should lead to more favourable clinical outcomes than deletions leading to fractional repeats. This primary factor could be further modulated by the presence or absence of a binding partner, the presence of specific SNPs that may slightly alter the function of the dystrophin protein or by factors modulating the expression such as microRNA or by SNPs. From a pragmatic point of view, our study should help caregivers to anticipate the clinical disease course in a patient carrying a given deletion based on the structure of the resulting truncated dystrophin. Exon skipping is a promising therapy that aims to convert the severe DMD into the milder BMD phenotype by skipping one or several exons in order to restore the reading-frame (28,64–66). Our work indicates that exon skipping will not produce a normal dystrophin and that some isoforms generated by this approach will be more functional than others. Indeed, restoring the reading-frame would not stabilize but rather slow down disease progression depending on the induced in-frame deletion. A better knowledge of the functionality of the different isoforms of dystrophin is thus of critical importance for predicting the extent of functional benefit that any given patient may have from the exon skipping strategy. It is worth mentioning that exon skipping aiming at generating a deletion of exons 45–51 could be also highly valuable for the most severe BMD deletions. Overall, preservation of repeat phasing is a critical determinant of functional outcome of newly synthetized proteins in patients that should be considered in various therapeutic approaches, in particular micro- or mini-dystrophin gene transfer strategies (28).

Materials and Methods

In silico analysis

Molecular homology modelling was used to generate models of the four truncated dystrophins to compare them with the wild-type R16–21 fragment previously obtained (67). For each truncated dystrophin, previously described models were used (18) and were lengthened by native repeats added at the C-terminal end (16).

MD was essentially performed similarly to our previous work (16). To simulate our systems with water and ions, we used the program NAMD 2.8 (68) and the CHARMM27 force field (69–72). The initial models were oriented along the *z*-axis and then solvated in rectangular water boxes generated using the *Solvate* plug-in of VMD (73). We thus ensured that there was a 25 Å thick layer of TIP3P water in the *x* directions and a 35 Å thick layer in the *y* and *z* direction. Subsequently, the VMD plug-in *Autoionize* was used to place ions randomly to neutralize the system. To adjust the position of the solvent (water and ions) around the molecules, each system was energy minimized for 10 000 steps using the conjugate gradient method while restraining the solute atoms with a 25 kcal mol^{-1} $Å^{-2}$ harmonic restraint.

The entire system (solvent and solute) was then subjected to another 10 000 steps of energy minimization to relieve any major stresses, followed by a slow heating to 310 K at constant volume over a period of 50 ps. The equilibration and production phases were performed for 40 ns for R16–21, 35 ns for Δ45–48 and 30 ns for the three other molecules applying periodic boundary conditions and using a 2 fs time step and the SHAKE algorithm. Van der Waals interactions were computed using a cut-off distance of 12 Å with a switching function starting at 10 Å, while long-range electrostatic forces were calculated using the particle-mesh Ewald method with a grid density of 1 $Å^{-3}$. To further reduce the cost of computing full electrostatics, a multiple-time-stepping procedure was employed to calculate long-range electrostatics every 4 fs. Berendsen baths were used to maintain the system temperature and pressure at 310 K and 1 atm, respectively.

The RMSD (in nm) compares the mean positions of the α-carbon atoms (Cα) of the peptide bond formed between the α-carboxyl group of one residue and the α-amino group of the next one in the protein (74). RMSD is used to measure the spatial deviation of all the Cα of the protein model during the time course of the MD compared with the initial model. It was calculated to determine the equilibration phase (i.e. when the RMSD becomes constant signifying that the model no more changes) and the last 22 ns of trajectories were kept for the analysis of all simulations (Supplementary Material, Fig. S1). The RMSF (in nm) reports the mean fluctuation of the position of each Cα during the MD trajectory. This indicates the sites which are highly dynamical (high RMSF) compared with sites which are rigid (low RMSF) (Supplementary Material, Fig. S2). To extract representative structures, the coordinate frames from the trajectory were clustered using the K-means algorithm. After testing different values, we chose to split the trajectory into three clusters (74). MHP were computed by the Platinum server (75,76) using the Ghose forcefield parameters. Electrostatic potentials were computed with the program APBS (68) using the Charmm forcefield and 50 mM concentrations for both sodium and chloride ions.

Biochemical analysis

Materials

The pGEX-4T-1 plasmid vector, GSTrap™ HP column were purchased from GE Healthcare. The *E. coli* BL21(DE3) bacteria were supplied by Invitrogen and restriction enzymes by New England Biolabs.

Cloning, expression and purification of proteins

The plasmid pTG11025 harbouring the cDNA for the Dp427 m muscle isoform of human dystrophin (NCBI Nucleotide Data Base NM-004006, provided by S. Braun Transgene, France) was used as a template for PCR amplification of fragments. The four truncated dystrophins resulting from deletions of exons 45–47, 45–48, 45–49 and 45–51 were introduced into a fragment of dystrophin recovering repeats R16–21 (Table 1). This choice was guided by the desire to maintain the same N- and C-terminal ends for all of the deletions and an entire repeat at each end, i.e. repeat 16 at the N-terminal end and repeat 21 at the C-terminal

end, even in the presence of internal deletions. The presence of the N- and C-terminal ends would be indispensable for maintaining the true folding of the fragment (77). The construct was generated by PCR and cloned into pGEX-4T-1 vector using *Bam*HI and *Xho*I restriction sites as previously described (25,67). For exon-deleted constructs, the exon 48/repeat 21 fragment to exon 52/repeat 21 fragment was generated by PCR amplification with an 'exon' primer including a *Bsp*TI restriction cassette at the 5′ end and R21 primer (see Supplementary Material, Table S1 for the primers). Products were cloned into the wild-type construct using *Bsp*TI (end of exon 44) and *Xho*I restriction sites, resulting in exon deletion. All the constructs were checked by a Big Dye terminator sequencing procedure. Recombinant proteins were expressed as GST-tagged proteins in the protease-deficient *E. coli* BL-21 strain. Cultures were performed at 37°C in LB medium supplemented with 50 µg/mL of ampicillin. The protein expression was induced by 0.5 mM IPTG addition for 4 h. Cells were harvested by centrifugation at 2500 *g* for 20 min.

The wild-type R16–21 was expressed as a soluble protein, whereas all truncated proteins were produced as inclusion bodies. All proteins were finally obtained as soluble forms after solubilization with *N*-lauryl-sarcosine (0.1%), affinity chromatography and further purification either with hydrophobic chromatography (RΔ45–47 and RΔ45–48) or not (RΔ45–49 and RΔ45–51). Exclusion chromatography performed at the end of the purification process showed that the proteins were all monomeric. Proteins were concentrated in a Tris 20 mM, pH 7.5, buffer containing NaCl 150 mM, EDTA 0.1 mM and glycerol 5% (TNEG buffer) using centrifugation-based concentrators and concentration was determined by spectroscopy at 280 nm and using theoretical molar extinction coefficients.

CD and fluorescence analysis of the purified proteins

CD was performed with a JASCO J-810 (Nantes, France) spectropolarimeter with protein concentration of ∼2.5 µM against the TNEG buffer. Spectra were acquired in the range 200–250 nm at 20°C with a path length of 0.2 cm. The percentage of α-helix was obtained using a 100% α-helix value of −36 000 deg cm^2 dmol^{-1} at 222 nm as previously described (78). Thermal unfolding was followed at 222 nm with temperature increase of 1 deg/min from 15 to 85°C. As partial refolding after heating at 70°C was observed showing that denaturation was reversible, CD signal was fitted to a two-state transition as previously described (78).

Tryptophan fluorescence spectra of the five proteins at 0.5 µM in TNE buffer were recorded on a Fluorolog spectrofluorimeter (Horiba Jobin-Yvon, Longjumeau, France) at 295 nm excitation wavelength at 20°C. After appropriate buffer correction, emission spectra of non-denatured proteins were obtained. Urea unfolding was performed by incubating proteins with urea from 0.5 to 8 M in TNEG buffer with 0.1 M steps for 2 h before fluorescence measurement. The maximum wavelength (λ_{max}) and the intensity of fluorescence were measured from the emission spectra. Reversibility of the denaturation was checked by 10-fold dilution of the 8 M urea-treated protein and by observing similar spectra of this diluted and native protein. The analysis of the denaturation was analysed as previously described (25).

Stopped-flow data were recorded on a stopped-flow BioLogic SFM-3, MOS 250 (Grenoble, France) device with a dead time of 2.2 ms. Proteins were diluted in 8 M urea 2 h before refolding measurements. As a first control, the urea denatured proteins were diluted 10-fold in TNE and their tryptophan fluorescence recorded. Each protein was able to refold with the same tryptophan fluorescence spectrum after renaturation, and therefore, the refolding after 8 M urea denaturation could be used to follow the refolding by stopped-flow fluorescence. The refolding reactions were initiated at 20°C by 10-fold dilution of the urea-treated proteins in TNEG buffer giving final protein concentrations of 0.25 µM. The time dependent of tryptophan fluorescence changes were monitored at excitation and emission wavelengths of 295 and 345 nm, respectively. Curves were derived from the averages of at least 10 individual kinetic data points after subtraction of the background urea buffer signal. The refolding rate constants were obtained by fitting the data with mono- or biexponential functions.

BMD patient cohort

This is a retrospective study using the national UMD-DMD France database (17) which collected data of DMD and BMD patients identified since >20 years. Two hundred and fifty-one BMD patients carrying one of the four in-frame deletions (Δ45–47, Δ45–48, Δ45–49 or Δ45–51) were retrieved from the database (Table 3). Only the patients older than 16 were further considered for the study. The comparison of disease severity between the four groups was based on two clinical criteria: the age of DCM onset (defined as the age when a left ventricular ejection fraction value ≤55% as determined by echocardiography was observed) and the age at permanent WC use. To avoid bias in our analysis, we did not include patients with non-permanent WC due to the difficulty in quantifying this criterion (duration of WC use, use inside or outside the home, maximal walking distance) from one patient to another. Overall, 106 patients had definite DCM and/or were WC users with the deletions Δ45–47, Δ45–48, Δ45–49 and 19 of which displayed both DCM and WC use (Supplementary Material, Table S2). No patient with DCM or WC dependency was found in the subgroup of three BMD patients with Δ45–51. Furthermore, we collected data of dystrophin WB analysis using DYS1, DYS2 and DYS3 antibodies (79) performed during the diagnostic approach for 47 over the 106 patients. A semi-quantitative evaluation by visual inspection of dystrophin expression level was done. For each patient, dystrophin amounts were compared with control muscle extracts in three conditions, no dilution and 1/2 and one-third dilutions. The levels were then visually categorized into four amount classes: normal (∼70–100% of control), high (∼50–70% of control), medium (∼10–50% of control) and low (<10% of control) (Supplementary Material, Table S2).

Supplementary Material

Supplementary Material is available at *HMG* online.

Acknowledgements

The authors thank all of the clinical and molecular contributors to the UMD-DMD France database, including other diagnostic laboratories (list available at http://umd.be/DMD/W_DMD/reseau_FR.html), and Dr Dominique Ménard and the NEMO network for their contributions to the collection of part of the clinical data. The authors acknowledge the technical contribution of Christophe Tascon to the biochemical work. The authors are grateful for Yann Le Cunff for statistical analyses of the clinical data. The authors gratefully acknowledge Kevin Flanigan for interesting and helpful discussions.

Conflict of Interest statement. None declared.

Funding

This work was supported by the 'Association Française contre les Myopathies' (grant 16810), Rennes Metropole (AIS grant) and the 'Grand Equipement National de Calcul Intensif' (GENCI) for access to the HPC resources of (TGCC/CINES/IDRIS) under the allocation of 2012–2013 (grant DYSIM 076816). A.N. was recipient of a 'Centre National de la Recherche Scientifique' fellowship.

References

1. Koenig, M., Hoffman, E.P., Bertelson, C.J., Monaco, A.P., Feener, C. and Kunkel, L.M. (1987) Complete cloning of the Duchenne muscular dystrophy (DMD) cDNA and preliminary genomic organization of the DMD gene in normal and affected individuals. *Cell*, **50**, 509–517.
2. Koenig, M., Beggs, A., Moyer, M., Scherpf, S., Heindrich, K., Bettecken, T., Meng, G., Muller, C., Lindlof, M. and Kaariainen, H. (1989) The molecular basis for Duchenne versus Becker muscular dystrophy: correlation of severity with type of deletion. *Am. J. Hum. Genet.*, **45**, 498–506.
3. Bushby, K.M., Thambyayah, M. and Gardner-Medwin, D. (1991) Prevalence and incidence of Becker muscular dystrophy. *Lancet*, **337**, 1022–1024.
4. Aartsma-Rus, A., Van Deutekom, J.C., Fokkema, I.F., Van Ommen, G.J. and Den Dunnen, J.T. (2006) Entries in the Leiden Duchenne muscular dystrophy mutation database: an overview of mutation types and paradoxical cases that confirm the reading-frame rule. *Muscle Nerve*, **34**, 135–144.
5. Mah, J.K., Korngut, L., Dykeman, J., Day, L., Pringsheim, T. and Jette, N. (2014) A systematic review and meta-analysis on the epidemiology of Duchenne and Becker muscular dystrophy. *Neuromuscul. Disord.*, **24**, 482–491.
6. Beggs, A., Hoffman, E., Snyder, J., Arahata, K., Specht, L., Shapiro, F., Angelini, C., Sugita, H. and Kunkel, L. (1991) Exploring the molecular basis for variability among patients with Becker muscular dystrophy: dystrophin gene and protein studies. *Am. J. Hum. Genet.*, **49**, 54–67.
7. Bushby, K.M. and Gardner-Medwin, D. (1993) The clinical, genetic and dystrophin characteristics of Becker muscular dystrophy. I. Natural history. *J. Neurol.*, **240**, 98–104.
8. Comi, G.P., Prelle, A., Bresolin, N., Moggio, M., Bardoni, A., Gallanti, A., Vita, G., Toscano, A., Ferro, M.T., Bordoni, A. *et al.* (1994) Clinical variability in Becker muscular dystrophy. Genetic, biochemical and immunohistochemical correlates. *Brain*, **117**, 1–14.
9. Bladen, C.L., Rafferty, K., Straub, V., Monges, S., Moresco, A., Dawkins, H., Roy, A., Chamova, T., Guergueltcheva, V., Korngut, L. *et al.* (2013) The TREAT-NMD Duchenne muscular dystrophy registries: conception, design, and utilization by industry and academia. *Hum. Mutat.*, **34**, 1449–1457.
10. Melacini, P., Fanin, M., Danieli, G.A., Fasoli, G., Villanova, C., Angelini, C., Vitiello, L., Miorelli, M., Buja, G.F., Mostacciuolo, M.L. *et al.* (1993) Cardiac involvement in Becker muscular dystrophy. *J. Am. Coll. Cardiol.*, **22**, 1927–1934.
11. Finsterer, J. and Stollberger, C. (2008) Cardiac involvement in Becker muscular dystrophy. *Can. J. Cardiol.*, **24**, 786–792.
12. Kaspar, R.W., Allen, H.D., Ray, W.C., Alvarez, C.E., Kissel, J.T., Pestronk, A., Weiss, R.B., Flanigan, K.M., Mendell, J.R. and Montanaro, F. (2009) Analysis of dystrophin deletion mutations predicts age of cardiomyopathy onset in becker muscular dystrophy. *Circ. Cardiovasc. Genet.*, **2**, 544–551.
13. Romfh, A. and McNally, E.M. (2010) Cardiac assessment in Duchenne and becker muscular dystrophies. *Curr. Heart Fail Rep.*, **7**, 212–218.
14. Koenig, M., Monaco, A.P. and Kunkel, L.M. (1988) The complete sequence of dystrophin predicts a rod-shaped cytoskeletal protein. *Cell*, **53**, 219–226.
15. Le Rumeur, E., Winder, S.J. and Hubert, J.F. (2010) Dystrophin: more than just the sum of its parts. *Biochim. Biophys. Acta*, **1804**, 1713–1722.
16. Legrand, B., Giudice, E., Nicolas, A., Delalande, O. and LeRumeur, E. (2011) Computational study of the human dystrophin repeats: interaction properties and molecular dynamics. *PLos ONE*, **6**, e23819.
17. Tuffery-Giraud, S., Beroud, C., Leturcq, F., Yaou, R.B., Hamroun, D., Michel-Calemard, L., Moizard, M.P., Bernard, R., Cossee, M., Boisseau, P. *et al.* (2009) Genotype-phenotype analysis in 2,405 patients with a dystrophinopathy using the UMD-DMD database: a model of nationwide knowledgebase. *Hum. Mutat.*, **30**, 934–945.
18. Nicolas, A., Lucchetti-Miganeh, C., Ben Yaou, R., Kaplan, J.C., Chelly, J., Leturcq, F., Barloy-Hubler, F. and Le Rumeur, E. (2012) Assessment of the structural and functional impact of in-frame mutations of the DMD gene, using the tools included in the eDystrophin online database. *Orphanet. J. Rare Dis.*, **7**, 45.
19. Menhart, N. (2006) Hybrid spectrin type repeats produced by exon-skipping in dystrophin. *Biochim. Biophys. Acta*, **1764**, 993–999.
20. Yokota, T., Duddy, W. and Patridge, T. (2007) Optimizing exon skipping therapies for DMD. *Acta Myolog.*, **26**, 179–184.
21. Winder, S.J., Gibson, T.J. and Kendrick-Jones, J. (1995) Dystrophin and utrophin: the missing links! *FEBS Lett.*, **369**, 27–33.
22. Laskowski, R.A., MacArthur, M.W., Moss, D.S. and Thornton, J.M. (1993) PROCHECK: a program to check the stereochemical quality of protein structures. *J. Appl. Cryst.*, **26**, 283–291.
23. Muthu, M., Richardson, K.A. and Sutherland-Smith, A.J. (2012) The crystal structures of dystrophin and utrophin spectrin repeats: implications for domain boundaries. *PLoS ONE*, **7**, e40066.
24. Legardinier, S., Raguénès-Nicol, C., Tascon, C., Rocher, C., Hardy, S., Hubert, J.F. and Le Rumeur, E. (2009) Mapping of the lipid-binding and stability properties of the central rod domain of human dystrophin. *J. Mol. Biol.*, **389**, 546–558.
25. Legardinier, S., Hubert, J.-F., Le Bihan, O., Tascon, C., Rocher, C., Raguénès-Nicol, C., Bondon, A., Hardy, S. and Le Rumeur, E. (2008) Sub-domains of the dystrophin rod domain display contrasting lipid-binding and stability properties. *Biochim. Biophys. Acta*, **1784**, 672–682.
26. Magri, F., Govoni, A., D'Angelo, M.G., Del Bo, R., Ghezzi, S., Sandra, G., Turconi, A.C., Sciacco, M., Ciscato, P., Bordoni, A. *et al.* (2011) Genotype and phenotype characterization in a large dystrophinopathic cohort with extended follow-up. *J. Neurol.*, **258**, 1610–1623.
27. Anthony, K., Cirak, S., Torelli, S., Tasca, G., Feng, L., Arechavala-Gomeza, V., Armaroli, A., Guglieri, M., Straathof, C.S., Verschuuren, J.J. *et al.* (2011) Dystrophin quantification and clinical correlations in Becker muscular dystrophy: implications for clinical trials. *Brain*, **134**, 3544–3556.
28. Jarmin, S., Kymalainen, H., Popplewell, L. and Dickson, G. (2014) New developments in the use of gene therapy to treat Duchenne muscular dystrophy. *Expert Opin. Biol. Ther.*, **14**, 209–230.
29. Wilton, S.D., Fletcher, S. and Flanigan, K.M. (2014) Dystrophin as a therapeutic biomarker: are we ignoring data from the past? *Neuromuscul. Disord.*, **24**, 463–466.
30. Morandi, L., Mora, M., Confalonieri, V., Barresi, R., Di Blasi, C., Brugnoni, R., Bernasconi, P., Mantegazza, R., Dworzak, F.,

Antozzi, C. et al. (1995) Dystrophin characterization in BMD patients: correlation of abnormal protein with clinical phenotype. J. Neurol. Sci., 132, 146–155.
31. van den Bergen, J.C., Schade van Westrum, S.M., Dekker, L., van der Kooi, A.J., de Visser, M., Wokke, B.H., Straathof, C.S., Hulsker, M.A., Aartsma-Rus, A., Verschuuren, J.J. et al. (2013) Clinical characterisation of Becker muscular dystrophy patients predicts favourable outcome in exon-skipping therapy. J. Neurol. Neurosurg. Psychiatry, 85, 92–98.
32. Bushby, K.M., Gardner-Medwin, D., Nicholson, L.V., Johnson, M.A., Haggerty, I.D., Cleghorn, N.J., Harris, J.B. and Bhattacharya, S.S. (1993) The clinical, genetic and dystrophin characteristics of Becker muscular dystrophy. II. Correlation of phenotype with genetic and protein abnormalities. J. Neurol., 240, 105–112.
33. van den Bergen, J.C., Wokke, B.H., Janson, A.A., van Duinen, S.G., Hulsker, M.A., Ginjaar, H.B., van Deutekom, J.C., Aartsma-Rus, A., Kan, H.E. and Verschuuren, J.J. (2014) Dystrophin levels and clinical severity in Becker muscular dystrophy patients. J. Neurol. Neurosurg. Psychiatry, 85, 747–753.
34. Aartsma-Rus, A. (2014) Dystrophin analysis in clinical trials. J. Neuromuscul. Dis., 1, 41–53.
35. Neri, M., Torelli, S., Brown, S., Ugo, I., Sabatelli, P., Merlini, L., Spitali, P., Rimessi, P., Gualandi, F., Sewry, C. et al. (2007) Dystrophin levels as low as 30% are sufficient to avoid muscular dystrophy in the human. Neuromuscul. Disord., 17, 913–918.
36. Carsana, A., Frisso, G., Tremolaterra, M.R., Lanzillo, R., Vitale, D.F., Santoro, L. and Salvatore, F. (2005) Analysis of dystrophin gene deletions indicates that the hinge III region of the protein correlates with disease severity. Ann. Hum. Genet., 69, 253–259.
37. Harper, S.Q., Hauser, M.A., DelloRusso, C., Duan, D., Crawford, R.W., Phelps, S.F., Harper, H.A., Robinson, A.S., Engelhardt, J.F., Brooks, S.V. et al. (2002) Modular flexibility of dystrophin: implications for gene therapy of Duchenne muscular dystrophy. Nat. Med., 8, 253–261.
38. England, S., Nicholson, L., Johnson, M., Forrest, S., Love, D., Zubrzycka-Gaarn, E., Bulman, D., Harris, J. and Davies, K. (1990) Very mild muscular dystrophy associated with the deletion of 46% of the dystrophin. Nature, 343, 180–182.
39. Ferrer, A., Foster, H., Wells, K.E., Dickson, G. and Wells, D.J. (2004) Long-term expression of full-length human dystrophin in transgenic mdx mice expressing internally deleted human dystrophins. Gene Ther., 11, 884–893.
40. Draviam, R.A., Wang, B., Li, J., Xiao, X. and Watkins, S.C. (2006) Mini-dystrophin efficiently incorporates into the dystrophin protein complex in living cells. J. Muscle Res. Cell Motil., 27, 53–67.
41. Wang, Z., Kuhr, C.S., Allen, J.M., Blankinship, M., Gregorevic, P., Chamberlain, J.S., Tapscott, S.J. and Storb, R. (2007) Sustained AAV-mediated dystrophin expression in a canine model of Duchenne muscular dystrophy with a brief course of immunosuppression. Mol. Ther., 15, 1160–1166.
42. Banks, G.B., Combs, A.C., Chamberlain, J.R. and Chamberlain, J.S. (2008) Molecular and cellular adaptations to chronic myotendinous strain injury in mdx mice expressing a truncated dystrophin. Hum. Mol. Genet., 17, 3975–3986.
43. Foster, H., Popplewell, L. and Dickson, G. (2012) Genetic therapeutic approaches for Duchenne muscular dystrophy. Hum. Gene Ther., 23, 676–687.
44. Henderson, D.M., Belanto, J.J., Li, B., Heun-Johnson, H. and Ervasti, J.M. (2011) Internal deletion compromises the stability of dystrophin. Hum. Mol. Genet., 20, 2955–2963.
45. Petrof, B.J., Shrager, J.B., Stedmann, H.H., Kelly, A.M. and Sweeney, H.L. (1993) Dystrophin protects the sarcolemma from stresses developed during muscle contraction. Proc. Natl. Acad. Sci. USA, 90, 3710–3714.
46. Deconinck, N. and Dan, B. (2007) Pathophysiology of Duchenne muscular dystrophy: current hypotheses. Pediatr. Neurol., 36, 1–7.
47. Nicolas, A., Delalande, O., Hubert, J.F. and Le Rumeur, E. (2014) The spectrin family of proteins: a unique coiled-coil fold for various molecular surface properties. J. Struct. Biol., 186, 392–401.
48. Helderman-van den Enden, A.T., Straathof, C.S., Aartsma-Rus, A., den Dunnen, J.T., Verbist, B.M., Bakker, E., Verschuuren, J.J. and Ginjaar, H.B. (2010) Becker muscular dystrophy patients with deletions around exon 51; a promising outlook for exon skipping therapy in Duchenne patients. Neuromuscul. Disord., 20, 251–254.
49. Amann, K.J., Renley, B.A. and Ervasti, J.M. (1998) A cluster of basic repeats in the dystrophin rod domain binds F-actin through an electrostatic interaction. J. Biol. Chem., 273, 28419–28423.
50. Ervasti, J.M. (2006) Dystrophin, its interactions with other proteins, and implications for muscular dystrophy. Biochim. Biophys. Acta, 1772, 108–117.
51. Schwartz, M., Duno, M., Palle, A.L., Krag, T. and Vissing, J. (2007) Deletion of exon 16 of the dystrophin gene is not associated with disease. Hum. Mutat., 28, 205.
52. Witting, N., Duno, M. and Vissing, J. (2011) Deletion of exon 26 of the dystrophin gene is associated with a mild Becker muscular dystrophy phenotype. Acta Myolog., 30, 182–184.
53. Lai, Y., Thomas, G.D., Yue, Y., Yang, H.T., Li, D., Long, C., Judge, L., Bostick, B., Chamberlain, J.S., Terjung, R.L. et al. (2009) Dystrophins carrying spectrin-like repeats 16 and 17 anchor nNOS to the sarcolemma and enhance exercise performance in a mouse model of muscular dystrophy. J. Clin. Invest., 119, 624–635.
54. Giudice, E., Molza, A.-E., Laurin, Y., Nicolas, A., Le Rumeur, E. and Delalande, O. (2013) Molecular clues to the dystrophin–nNOS interaction: a theoretical approach. Biochemistry, 52, 7777–7784.
55. Beroud, C., Tuffery-Giraud, S., Matsuo, M., Hamroun, D., Humbertclaude, V., Monnier, N., Moizard, M.P., Voelckel, M.A., Calemard, L.M., Boisseau, P. et al. (2007) Multiexon skipping leading to an artificial DMD protein lacking amino acids from exons 45 through 55 could rescue up to 63% of patients with Duchenne muscular dystrophy. Hum. Mutat., 28, 196–202.
56. Gentil, C., Leturcq, F., Ben Yaou, R., Kaplan, J.C., Laforet, P., Penisson-Besnier, I., Espil-Taris, C., Voit, T., Garcia, L. and Pietri-Rouxel, F. (2012) Variable phenotype of del45–55 Becker patients correlated with nNOSmu mislocalization and RYR1 hypernitrosylation. Hum. Mol. Genet., 21, 3449–3460.
57. Dwianingsih, E.K., Malueka, R.G., Nishida, A., Itoh, K., Lee, T., Yagi, M., Iijima, K., Takeshima, Y. and Matsuo, M. (2014) A novel splicing silencer generated by DMD exon 45 deletion junction could explain upstream exon 44 skipping that modifies dystrophinopathy. J. Hum. Genet., 59, 423–429.
58. Flanigan, K.M., Dunn, D.M., von Niederhausern, A., Soltanzadeh, P., Gappmaier, E., Howard, M.T., Sampson, J.B., Mendell, J.R., Wall, C., King, W.M. et al. (2009) Mutational spectrum of DMD mutations in dystrophinopathy patients: application of modern diagnostic techniques to a large cohort. Hum. Mutat., 30, 1657–1666.
59. Cacchiarelli, D., Incitti, T., Martone, J., Cesana, M., Cazzella, V., Santini, T., Sthandier, O. and Bozzoni, I. (2011) miR-31

modulates dystrophin expression: new implications for Duchenne muscular dystrophy therapy. *EMBO Rep.*, **12**, 136–141.
60. Kerst, B., Mennerich, D., Schuelke, M., Stoltenburg-Didinger, G., von Moers, A., Gossrau, R., van Landeghem, F.K., Speer, A., Braun, T. and Hubner, C. (2000) Heterozygous myogenic factor 6 mutation associated with myopathy and severe course of Becker muscular dystrophy. *Neuromuscul. Disord.*, **10**, 572–577.
61. Davis, D.B., Delmonte, A.J., Ly, C.T. and McNally, E.M. (2000) Myoferlin, a candidate gene and potential modifier of muscular dystrophy. *Hum. Mol. Genet.*, **9**, 217–226.
62. Pegoraro, E., Hoffman, E.P., Piva, L., Gavassini, B.F., Cagnin, S., Ermani, M., Bello, L., Soraru, G., Pacchioni, B., Bonifati, M.D. *et al.* (2011) SPP1 genotype is a determinant of disease severity in Duchenne muscular dystrophy. *Neurology*, **76**, 219–226.
63. Bello, L., Piva, L., Barp, A., Taglia, A., Picillo, E., Vasco, G., Pane, M., Previtali, S.C., Torrente, Y., Gazzerro, E. *et al.* (2012) Importance of SPP1 genotype as a covariate in clinical trials in Duchenne muscular dystrophy. *Neurology*, **79**, 159–162.
64. Aartsma-Rus, A. (2010) Antisense-mediated modulation of splicing: therapeutic implications for Duchenne muscular dystrophy. *RNA Biol.*, **7**, 453–461.
65. Hoffman, E.P. and Connor, E.M. (2013) Orphan drug development in muscular dystrophy: update on two large clinical trials of dystrophin rescue therapies. *Discov. Med.*, **16**, 233–239.
66. Fairclough, R.J., Wood, M.J. and Davies, K.E. (2013) Therapy for Duchenne muscular dystrophy: renewed optimism from genetic approaches. *Nat. Rev. Genet.*, **14**, 373–378.
67. Ameziane-Le Hir, S., Raguénès-Nicol, C., Paboeuf, G., Nicolas, A., Chéron, A., Le Rumeur, E. and Vié, V. (2014) Cholesterol favors higher level of insertion and organization of spectrin-like repeat 16-21 of human dystrophin in membrane. *Biochim. Biophys. Acta*, **1838**, 1266–1273.
68. Phillips, J.C., Braun, R., Wang, W., Gumbart, J., Tajkhorshid, E., Villa, E., Chipot, C., Skeel, R.D., Kale, L. and Schulten, K. (2005) Scalable molecular dynamics with NAMD. *J. Comput. Chem.*, **26**, 1781–1802.
69. Felsenstein, J. (1987) Estimation of hominoid phylogeny from a DNA hybridization data set. *J. Mol. Evol.*, **26**, 123–131.
70. Baker, N.A., Sept, D., Joseph, S., Holst, M.J. and McCammon, J. A. (2001) Electrostatics of nanosystems: application to microtubules and the ribosome. *Proc. Natl. Acad. Sci. USA*, **98**, 10037–10041.
71. Mackerell, A.D., Bashford, D., Bellott, M., Dunbrack, R.L. Jr, Evanseck, J., Field, M.J., Fischer, S., Gao, J., Guo, H., Ha, S. *et al.* (1998) All atom empirical potential for molecular modeling and dynamics studies of protein. *J. Phys. Chem. B*, **102**, 3586–3615.
72. Foloppe, N. and Mackerell, A.D. Jr. (2000) Parameter optimization based on small molecule and condensed phase macromolecular target. *J. Comput. Chem.*, **21**, 86–104.
73. MacKerell, A.D. Jr and Banavali, N. (2000) Application to molecular dynamics simulations of DNA and RNA in solution. *J. Comput. Chem.*, **21**, 105–120.
74. Mackerell, A.D. Jr, Feig, M. and Brooks, C.L. 3rd (2004) Extending the treatment of backbone energetics in protein force fields: limitations of gas-phase quantum mechanics in reproducing protein conformational distributions in molecular dynamics simulations. *J. Comput. Chem.*, **25**, 1400–1415.
75. Efremov, R.G., Chugunov, A.O., Pyrkov, T.V., Priestle, J.P., Arseniev, A.S. and Jacoby, E. (2007) Molecular lipophilicity in protein modeling and drug design. *Curr. Med. Chem.*, **14**, 393–415.
76. Pyrkov, T.V., Chugunov, A.O., Krylov, N.A., Nolde, D.E. and Efremov, R.G. (2009) PLATINUM: a web tool for analysis of hydrophobic/hydrophilic organization of biomolecular complexes. *Bioinformatics*, **25**, 1201–1202.
77. Kahana, E. and Gratzer, W.B. (1995) Minimum folding unit of dystrophin rod domain. *Biochemistry*, **34**, 8110–8114.
78. Legardinier, S., Legrand, B., Raguénès-Nicol, C., Bondon, A., Hardy, S., Tascon, C., Le Rumeur, E. and Hubert, J.F. (2009) A two amino-acid mutation encountered in Duchenne muscular dystrophy decreases stability of the R23 spectrin-like repeat of dystrophin. *J. Biol. Chem.*, **284**, 8822–8832.
79. Anderson, L.V. and Davison, K. (1999) Multiplex Western blotting system for the analysis of muscular dystrophy proteins. *Am. J. Pathol.*, **154**, 1017–1022.